

1 **SLOPE-FAN DEPOSITIONAL ARCHITECTURE FROM HIGH-RESOLUTION**  
2 **FORWARD STRATIGRAPHIC MODELS**

3 **Nicolas Hawie<sup>1</sup>, Jacob A. Covault<sup>2</sup>, Dallas Dunlap<sup>2</sup>, and Zoltán Sylvester<sup>2</sup>**

4 *<sup>1</sup>Beicip Franlab, Rueil-Malmaison, France*

5 *<sup>2</sup>Bureau of Economic Geology, Jackson School of Geoscience, The University of Texas at Austin,*  
6 *Austin, TX, USA*

7  
8 **ABSTRACT**

9 Submarine fans in tectonically active continental-slope basins are targets of petroleum  
10 exploration and production. These slope fans commonly comprise compensationally stacked sandy  
11 and muddy architectural elements, including mass-transport deposits, weakly confined to  
12 distributary channel-and-lobe deposits, and leveed-channel deposits. The lateral continuity and  
13 vertical connectivity of these architectural elements are important uncertainties in reservoir  
14 characterization that influence fluid-flow behavior during hydrocarbon production. Here, we use  
15 a simple forward stratigraphic model to simulate the stratigraphic patterns and illuminate the likely  
16 distribution of fine-scale, sub-seismic heterogeneity in a slope fan. We used published seismic-  
17 reflection horizons from the tectonically active Columbus basin, offshore Trinidad, to define the  
18 top and base of a Pleistocene submarine fan. We then simulated the stratigraphic evolution of the  
19 slope fan with a series of DionisosFlow<sup>TM</sup> forward stratigraphic models. All variables were kept  
20 constant during the simulations in order to test the hypothesis that the autogenic evolution of the  
21 surface topography alone, as a result of erosion and deposition, can produce compensational-  
22 stacking patterns common in submarine fans. A reference-case model is similar to the thickness  
23 trend of published isochron maps of the Trinidad slope fan. The reference-case model also

24 produced patterns of compensational stacking. Varying the time step impacts the heterogeneity of  
25 the model. Shorter time steps are characterized by less sediment accumulation, which results in  
26 less sediment diversion during the subsequent time step, more gradual migration of channel  
27 deposits, shorter offset distances of depocenters, and shorter length-scale heterogeneity compared  
28 to longer time steps. Thus, a key characteristic of slope-fan deposits is autogenic compensational  
29 stacking, without any external forcing, which governs heterogeneity in these reservoirs.  
30 Furthermore, our results suggest that relatively simple diffusion-based models can produce  
31 realistic compensation patterns and future work will be focused on higher-resolution model  
32 calibration to seismic-reflection data and the influence of input variables on heterogeneity of  
33 channel-and-lobe deposits of slope fans.

34

## 35 **INTRODUCTION**

36 Submarine fans are depositional sinks of continental-margin sediment-routing systems,  
37 where they host stratigraphic archives of Earth history and environmental changes (Clift and  
38 Gaedicke, 2002; Fildani and Normark, 2004; Covault et al., 2010; 2011; Fildani et al., 2016).  
39 Submarine fans are also important reservoirs of natural resources (Pettingill and Weimer, 2002).  
40 Early models characterized submarine fans as laterally extensive sheets in cross section with  
41 radial- or cone-like depositional morphologies in map view across unconfined basin floors of low  
42 relief and with gentle gradients (e.g., Shepard and Emery, 1941; Dill et al., 1954; Menard, 1955;  
43 Heezen et al., 1959; Bouma et al., 1985) (Fig. 1). However, receiving-basin geometry and tectonic  
44 deformation can influence the organization of sandy and muddy architectural elements of  
45 submarine fans (Piper and Normark, 2001). For example, tectonically active slope basins and  
46 stepped slopes with abrupt changes in gradient commonly consist of ponded mass-transport

47 deposits overlain by weakly confined to distributary channel-and-lobe deposits, which transition  
48 to perched, downstream-thinning wedges comprising leveed-channel deposits (Beaubouef and  
49 Friedmann, 2000; Brami et al., 2000; Beaubouef et al., 2003; Prather, 2003) (Fig. 1); although,  
50 mass-transport deposits and leveed channels are not always present (e.g., Jobe et al., 2017). Such  
51 tectonically active slopes are targets of petroleum exploration and production (e.g., the slope basins  
52 and stepped slopes of the Gulf of Mexico and the Niger Delta; Damuth, 1994; Pirmez et al., 2000;  
53 Sullivan et al., 2004; Prather, 2003; Rowan et al., 2004; Adeogba et al., 2005; Deptuck et al., 2012;  
54 Sylvester et al., 2012).

55         Models of slope-fan stratigraphic architecture and evolution are predominantly based on  
56 insights from shallow-subsurface three-dimensional (3-D) seismic-reflection data (up to ~200 Hz  
57 peak frequency), with limited core penetrations (e.g., Beaubouef et al., 2003). These datasets can  
58 constrain the 3-D geometry of packages of strata as thin as several to tens of meters in the  
59 subsurface, but they lack the depth of penetration and deep-time perspective of conventional  
60 industry seismic-reflection data (e.g., generally <40 Hz peak frequency; Normark et al., 1993;  
61 Prather et al., 2012). Moreover, core calibration is limited and does not provide a strong 3-D  
62 lithologic control, which can be of importance to the spatial variation in properties in oil and gas  
63 reservoirs (i.e., heterogeneity; Lake and Jensen, 1989). These datasets provide insights into the  
64 compensational stacking of architectural elements and the stratigraphic evolution from ponded to  
65 perched fan deposits. However, an important uncertainty is the lateral continuity and vertical  
66 connectivity of sandy and muddy architectural elements at higher resolution. These architectural  
67 elements control the static and dynamic connectivity of slope-fan reservoirs and influence fluid-  
68 flow behavior during hydrocarbon production (e.g., Glenton et al., 2013; Sutton et al., 2013).

69           Deptuck et al. (2008) used high-resolution 2-D seismic-reflection profiles (900-7000 Hz  
70 frequencies) and piston cores to investigate the causes of heterogeneity in Pleistocene submarine  
71 fans offshore East Corsica. This work provided new details of the hierarchical levels of  
72 compensational stacking of deposits: individual beds stack to form lobe architectural elements,  
73 which stack to form more composite submarine fans. However, the high-resolution 2-D imagery  
74 of the Pleistocene deposits offshore East Corsica lacks the 3-D perspective of fan geometry.  
75 Physical experiments provide high temporal- and spatial-resolution insights into the  
76 morphodynamic processes of sediment-gravity flows and fans (e.g., Spinewine et al., 2009; Hoyal  
77 et al., 2011; 2014; Fernandez et al., 2014; Hamilton et al., 2015; Postma et al., 2016); however,  
78 these studies lack the long-term ( $>10^3$  yr) perspective of stratigraphic evolution and the complexity  
79 of field-scale depositional elements. Nevertheless, physical experiments offer the opportunity to  
80 constrain fundamental processes that operate in slope depositional environments when combined  
81 with other approaches, such as 3-D seismic-stratigraphic interpretation and forward stratigraphic  
82 modeling.

83           Forward stratigraphic modeling can provide insights into the long-term ( $>10^3$  yr)  
84 stratigraphic evolution of slope fans at high temporal and spatial resolution (e.g., Miller et al.,  
85 2008; Sun et al., 2010). Here, we evaluate the efficacy of a simple forward stratigraphic model to  
86 simulate the stratigraphic patterns and illuminate the fine-scale, sub-seismic heterogeneity of a  
87 slope fan. We used published seismic-reflection horizons from the Columbus basin, offshore  
88 Trinidad, to define the top and base of a Pleistocene submarine fan in a tectonically active slope.  
89 We then simulated the stratigraphic evolution of the slope fan with a series of DionisosFlow™  
90 forward stratigraphic models. All variables are kept constant during the simulations to test the  
91 hypothesis that the autogenic evolution of the surface topography alone, without any external

92 forcing, can produce the compensational-stacking patterns common to submarine fans (e.g.,  
93 Deptuck et al., 2008). We test the sensitivity of the models to time step (20 kyr, 10 kyr, 5 kyr, and  
94 1 kyr), and discuss the impact of varying the time step on the lateral continuity and vertical  
95 connectivity of sandy and muddy architectural elements in slope fans. These interpretations inform  
96 the prediction of 3-D sub-seismic heterogeneity of slope fans and demonstrate the value of  
97 integrated subsurface characterization and forward stratigraphic modeling to understand the range  
98 of reservoir connectivity and quality in such settings.

99

## 100 **GEOLOGIC SETTING AND PREVIOUS WORK**

101         The Columbus foreland-basin system, offshore eastern Trinidad, was created as a result of  
102 oblique subduction of the South American plate beneath the eastward migrating Caribbean plate  
103 since the Miocene (Leonard, 1983; Weber et al., 2001; Huyghe et al., 2004; Garciacaro et al.,  
104 2011a; 2011b) (Fig. 2). Transpression along the Central Range fault zone created a fold-thrust belt  
105 in Trinidad (Escalona and Mann, 2011). The offshore expression of the Central Range fault zone  
106 is the northwest-southeast-oriented Darien ridge, which defines the boundary between the  
107 Columbus basin and the Barbados accretionary wedge on the slope offshore of eastern Trinidad  
108 (Wood and Mize-Spansky, 2009; Moscardelli et al., 2012) (Fig. 3). The Darien ridge and related  
109 fold-thrust structures form highs on the present-day seafloor that locally exhibit >100 m of relief  
110 (Garciacaro et al., 2011a; 2011b; Moscardelli et al., 2012). Fold-thrust-belt deformation and  
111 tectono-sedimentary loading of Miocene-Pliocene sediment from the Orinoco river-delta system  
112 promoted mud diapirism and the development of northeast-southwest-oriented mud-volcano  
113 ridges on the seafloor (up to several hundreds of meters of relief) and shallow subsurface of the  
114 slope offshore of eastern Trinidad (Sullivan, 2005; Garciacaro et al., 2011a; 2011b; Moscardelli et

115 al., 2012). High-relief fold-thrust structures and mud volcanoes influence the pathways of down-  
116 slope sediment dispersal and the resulting stratigraphic architecture of mass-transport deposits and  
117 submarine canyon-channel-fan systems offshore of eastern Trinidad (Brami et al., 2000;  
118 Moscardelli et al., 2006; Wood and Mize-Spansky, 2009) (Figs. 3 and 4). Northwest-southeast-  
119 trending normal faults dominate the Columbus basin shelf and upper slope and accommodate local  
120 depocenters (Moscardelli et al., 2006).

121 We used published seismic-reflection horizons from the tectonically active slope east of  
122 the Columbus basin and along the southern margin of the Barbados accretionary wedge (the ‘NW’  
123 depocenter between the Darien and Haydn ridges in block 25A offshore of Trinidad; Brami et al.,  
124 2000; Wood and Mize-Spansky, 2009) to define the top and base of a submarine fan (Fig. 4). The  
125 seismic-reflection volume in block 25A is part of a set of volumes spanning nearly 11,000 km<sup>2</sup>  
126 that has been published in peer-reviewed literature by the Quantitative Clastics Laboratory at the  
127 Bureau of Economic Geology, the University of Texas at Austin (e.g., Moscardelli et al., 2006;  
128 Moscardelli and Wood, 2008; Wood and Mize-Spansky, 2009; Garciacaro et al., 2011b) (Fig. 3).  
129 The seismic-reflection dataset is also the subject of unpublished MS theses at the University of  
130 Texas at Austin (e.g., Mize, 2004; Sullivan, 2005). Exploration drilling in block 25A (Haydn-1  
131 well) revealed a thick section (>3 km) of Pliocene-Pleistocene slope-fan deposits (Patterson et al.,  
132 2001) (Fig. 2).

133 Moscardelli et al. (2006) interpreted the seismic-reflections immediately above their ‘2’  
134 and ‘1’ horizons to be Pleistocene mass-transport deposits at the base of the shallowest  
135 depositional sequence in block 25A. Brami et al. (2000) and Moscardelli et al. (2006) interpreted  
136 leveed-channel deposits of a slope fan between the top of the mass-transport deposits and the  
137 seafloor (Fig. 4). However, the low resolution of the 3-D seismic-reflection data in block 25A

138 prevented the mapping of individual channel-and-lobe architectural elements of the slope fan  
139 (tuning thickness >10 m based on frequency of 30-40 Hz and velocity of 1500-2000 m/s in the  
140 shallow subsurface). Individual channel-and-lobe architectural elements can be thinner than the  
141 tuning thickness of the seismic-reflection data (for dimensions of channel and lobe architectural  
142 elements, see Prélat et al., 2010; and McHargue et al., 2011). Wood and Mize-Spansky (2009)  
143 interpreted a leveed-channel system at the top of the depositional sequence, on the seafloor (Fig.  
144 4b). This channel system might extend hundreds of km across the tectonically active slope to the  
145 toe of the Barbados accretionary wedge and the Atlantic abyssal plain (Huyghe et al., 2004; Wood  
146 and Mize-Spansky, 2009) (Fig. 2).

147 Previous work has failed to document the stacking patterns of architectural elements of the  
148 slope fan in block 25A, and we predict compensational stacking of channel-and-lobe deposits  
149 based on previously documented growth patterns of submarine fans (e.g., Deptuck et al., 2008).  
150 We evaluate our prediction of compensational stacking with a series of DionisosFlow<sup>TM</sup> forward  
151 stratigraphic models, which also provide insights into the expected sub-seismic hierarchical  
152 structure of slope fans.

153

## 154 **METHODS**

### 155 **Forward Stratigraphic Modeling**

156 DionisosFlow<sup>TM</sup> software is a four dimensional process-based deterministic multi-  
157 lithology forward stratigraphic model that simulates basin filling (Granjeon, 1997; Granjeon and  
158 Joseph, 1999; Granjeon, 2014). A range of sedimentary processes are modeled including diffusive  
159 sediment transport, delta autoretreat, incision, large-scale avulsion, and slope failure in response  
160 to tectonic, climate, and sea-level fluctuations during millennia and longer time scales (e.g.,

161 Pinheiro-Moreira, 2000; Rabineau et al., 2005; Alzaga-Ruiz et al., 2009; Gvirtzman et al., 2014;  
162 Harris et al., 2016; Hawie et al., 2017). Detailed fluid dynamics are not considered in this model;  
163 the goal is to simulate the large-scale ( $10^2$ - $10^3$  m cell size) and long-term ( $10^3$ - $10^5$  yr time steps)  
164 evolution of basin fill.

165 Sediment transport equations are used to simulate the transport of various classes of  
166 sediment grain size (e.g., clay and sand) across a basin. This stratigraphic model combines 1) linear  
167 slope-driven diffusion (transport proportional to slope), referred to as hillslope creep, and 2) non-  
168 linear water- and slope-driven diffusion, referred to as water-discharge-driven transport  
169 (Willgoose et al., 1991; Tucker and Slingerland, 1994; Granjeon, 1997; Granjeon and Joseph,  
170 1999; Deville et al., 2015):

$$171 \quad Q_s = -(K_s/\vec{\nabla}h + K_w Q_w^m S^n)$$

172 where  $Q_s$  is sediment discharge ( $\text{km}^3/\text{Myr}$ ),  $K_s$  and  $K_w$  are the slope- and water-driven  
173 diffusion coefficients, respectively ( $\text{km}^2/\text{kyr}$ ),  $Q_w$  is water discharge ( $\text{m}^3/\text{s}$ ),  $n$  and  $m$  are exponents  
174 that affect sediment transport capacity with values between 1 and 2 (Tucker and Slingerland,  
175 1994),  $S$  is the dimensionless local gradient of the basin, and  $h$  (m) is topographic elevation  
176 (Granjeon, 2014). Sedimentation and erosion rates are quantified by a mass balance equation in 3-  
177 D for each class of grain size (Euzen et al., 2004). Sediment-gravity flows, commonly turbidity  
178 currents, are the primary agents of sediment transport, erosion, and deposition in submarine fans  
179 and related turbidite systems (Bouma et al., 1985). We liken the water-driven diffusion coefficient  
180 and the water discharge to a sediment-gravity-flow-driven diffusion coefficient and gravity-flow  
181 discharge, respectively, which govern the rate of sediment transport through the system. We have  
182 tuned the variables of the diffusion equation, including the gravity-flow-driven diffusion



183 coefficient and gravity-flow discharge, to achieve a thickness trend that is similar to the published  
184 seismic-stratigraphic interpretation in a reference-case model.

185

## 186 **Model Framework**

187         The goals of the modeling were to assess the impact of duration of time step (20 kyr, 10  
188 kyr, 5 kyr, and 1 kyr), flow properties, and seafloor topography on the size, shape, and sub-seismic  
189 stacking and heterogeneity of leveed-channel and lobe architectural elements of a slope fan. We  
190 modeled a reference case for a late Pleistocene period during the last glacial cycle (124.5-24.5 ka)  
191 within a bounding box of 17 km x 17 km with cell sizes of 200 m x 200 m and an initial simulated  
192 time step of 10 kyr (Table 1). The down-dip model boundary was set as open to allow sediment  
193 transport outside of the model domain. Deville et al. (2015) recently used DionisosFlow™ to  
194 model large-scale sediment fairways and facies distribution of submarine fans (1200 km x 1200  
195 km area; 10 km x 10 km grid size). However, this is the first high-resolution DionisosFlow™  
196 forward stratigraphic model of a slope fan with a 300-600 m-wide feeder channel at sub-seismic  
197 resolution, using grain sizes ranging from sand to clay. We used the regional surface at the base of  
198 the slope fan, which overlies mass-transport deposits mapped by Moscardelli et al. (2006), as the  
199 initial bathymetry of the model (Fig. 4a). The feeder channel is in the south based on published  
200 seismic-stratigraphic interpretations (Brami et al., 2000; Moscardelli et al., 2006; Moscardelli and  
201 Wood, 2008; Wood and Mize-Spansky, 2009).

202         We did not account for differential subsidence in the model. The transport parameters  
203 used for the reference case model range from 10-100 km<sup>2</sup>/kyr for water-driven diffusion (or, in  
204 the case of submarine fans, sediment-gravity-flow-driven diffusion;  $K_w$ ) and 0.001-0.1 km<sup>2</sup>/kyr  
205 for slope-driven transport ( $K_s$ ) (Table 1). We determined these ranges of diffusion coefficients

206 based on simplifying the diffusion equation to  $Q_s = K_w Q_w S$  and solving for  $K_w$  based on  $Q_s$ ,  $Q_w$ ,  
207 and  $S$  from the Trinidad slope-fan system. The slope-driven diffusion coefficient ( $K_s$ ) is  
208 relatively small, several orders of magnitude less than the water-driven diffusion coefficient ( $K_w$ )  
209 (Flemings and Jordan, 1989; Avouac and Burov, 1996). For our depositional system, slope-  
210 driven diffusion has less impact on model results compared to the water-driven diffusion  
211 coefficient ( $K_w$ ) because of very small gradients of the basin floor. These parameters are within  
212 the lower order of magnitude of Deville et al. (2015), who modeled a complete source-to-sink  
213 system. Ratios of diffusion coefficients are applied to different grain sizes (Table 1) (Granjeon,  
214 1997; Granjeon and Joseph 1999; Euzen et al., 2004; Granjeon 2014). Following the reference-  
215 case model calibration, we tested the sensitivity of the models to time step (20 kyr, 5 kyr, and 1  
216 kyr). It is important to note that we attempted to generate model results that captured the gross  
217 geometry (i.e., thickness trend) and sub-seismic-scale stratigraphic architecture of the channel-  
218 and-lobe deposits of the slope fan offshore of Trinidad. In the future, we will attempt to generate  
219 a high-resolution model calibration to published seismic-stratigraphic interpretations of the slope  
220 fan.

221

## 222 **RESULTS**

223 For the reference case (i.e., 10 kyr time step), sediment was transported to the north along  
224 a gentle regional slope ( $<0.5^\circ$ ) and diverted around locally rugose topography of underlying mass-  
225 transport deposits and mud volcanoes (Fig. 5). The model output shows at least four major phases  
226 of sediment diversion during the migration of a relatively coarse-grained depocenter. Initially, the  
227 depocenter was oriented southwest-to-northeast (0.124-0.084 Ma), then it shifted to the west and  
228 was oriented more south-to-north (0.084-0.064 Ma), then it split into two concomitant depocenters

229 (0.064-0.034 Ma) and, finally, it returned to a southwest-to-northeast orientation (0.034-0.024 Ma)  
230 (Fig. 5; Supplementary Files 1 and 2). These phases of sediment diversion reflect compensational  
231 stacking in response to the construction of depositional topography. Moreover, the overall  
232 proximal-to-distal thickness trend of the model follows the isochron map tendency of the Trinidad  
233 slope fan (Fig. 5), although the proximal part of the model is thicker (Fig. 5c). At this stage in our  
234 modeling effort, the thickness difference is likely a result of the challenge of simulating significant  
235 sediment bypass with the limited processes used in this simplistic diffusion-based model. In the  
236 future, we will attempt higher-resolution calibrations to the seismic-reflection-based  
237 interpretation. While the seismic-stratigraphic interpretation can provide insights into the general  
238 thickness trends in the subsurface, the reference-case forward stratigraphic model also shows  
239 plausible patterns of lateral and vertical distribution of grain sizes. A proximal-to-distal  
240 architectural trend is also apparent; the proximal reach of the model shows multiple  
241 compensationally stacked, relatively confined, coarse-grained leveed-channel deposits (several km  
242 wide), which transition distally to unconfined, finer-grained lobe deposits (~4 km wide) (Fig. 5f).

243 Varying the simulated time step (20 kyr, 5 kyr, and 1 kyr) resulted in a similar thickness  
244 trend and compensational stacking of depocenters as the reference-case model (Fig. 6;  
245 Supplementary Files 3-8). In particular, all models show three to four major phases of sediment  
246 diversion during the migration of a relatively coarse-grained depocenter (Fig. 6; Supplementary  
247 Files 3-8). Moreover, the overall proximal-to-distal trend from relatively coarse-grained leveed-  
248 channel to finer-grained lobe deposits is similar in all models (Fig. 6). However, the detailed 3-D  
249 heterogeneity varies between models. In the 20 kyr time-step model, ~4-5 discrete packages of  
250 proximal leveed-channel deposits are several km wide and expand and thin downstream to >5 km-  
251 wide distal lobe deposits (Fig. 6a). Grain size is consistent over several hundreds of m to several

252 km. The vertical resolution of the model is lower than the reference-case model (of the order of  
253  $10^1$  m-thick accumulations of sediment per time step). This is because sediment supply was kept  
254 constant in all simulations; therefore, longer time steps will produce thicker accumulations of  
255 sediment per time step. In the 5 kyr time-step model, more numerous (as many as 8-10) packages  
256 of leveed-channel deposits are  $\sim 2$  km wide and expand and thin downstream to  $<4$  km-wide distal  
257 lobe deposits (Fig. 6b). Grain size is consistent over several hundreds of m to approximately a km.  
258 The vertical resolution of the model is high, with accumulations of sediment per time step of the  
259 order of  $10^0$  m, which provides finer-scale perspectives of more frequent compensational stacking  
260 and the 3-D interstratification of sand and clay in distal lobe deposits. In the 1 kyr time-step model,  
261  $>15$  packages of leveed-channel deposits are  $\sim 1$ -2 km wide and expand and thin downstream to 2-  
262 4 km wide distal lobe deposits (Fig. 6c). Grain size varies rapidly over several hundreds of m and  
263 the vertical resolution of the model is high (of the orders of  $10^{-1}$ - $10^0$  m-thick accumulations of  
264 sediment per time step). In this 1 kyr time-step model, the 3-D heterogeneity is at a resolution  
265 observed in outcropping submarine fans (e.g., Mutti and Normark, 1987; Sullivan et al., 2000;  
266 2004; Prélat et al., 2009).

267 Even though all models show similar patterns of compensational stacking, from a  
268 qualitative perspective, shorter time steps result more gradual migration of channel deposits,  
269 shorter offset distances of depocenters, and shorter length-scale heterogeneity compared to longer  
270 time steps. This is because less sediment accumulates during shorter time steps and, as a result,  
271 less sediment diversion during the subsequent time step is expected as the relatively coarse-grained  
272 depocenter migrates around the model domain. In contrast, more sediment accumulates during  
273 longer time steps, resulting in a thicker deposit, which generates steeper gradients and longer offset

274 distances of depocenters. Thus, the controls on the compensational stacking and depocenter  
275 evolution are autogenic in these models.

276

## 277 **DISCUSSION**

### 278 **Slope-Fan Depositional Model**

279         The stratigraphic evolution of the depositional sequence offshore of Trinidad is similar to  
280 other systems in tectonically active slopes (e.g., the Gulf of Mexico and the Niger Delta;  
281 Beaubouef and Friedmann, 2000; Beaubouef et al., 2003; Prather, 2003; Adeogba et al., 2005;  
282 Deptuck et al., 2012); in slope basins and stepped slopes with abrupt changes in gradient, mass-  
283 transport deposits are overlain by weakly confined channel-and-lobe and leveed-channel deposits  
284 of a submarine fan (Brami et al., 2000; Moscardelli et al., 2006; Wood and Mize-Spansky, 2009)  
285 (Fig. 1). The sub-seismic-scale stratigraphic architecture of the channel-and-lobe deposits of the  
286 slope fan offshore of Trinidad reflects stacking and depositional processes simulated in other  
287 forward stratigraphic models, such as repeated cycles of channel avulsion, compensational  
288 stacking, and unconfined deposition at the mouths of channels (e.g., Sun et al., 2010).  
289 Compensational stacking is a key characteristic of submarine lobe deposits (e.g., Deptuck et al.,  
290 2008; Jobe et al., 2017), and our results suggest that relatively simple diffusion-based models can  
291 produce realistic compensation patterns. We interpret that the depositional sequence in block 25A  
292 offshore of Trinidad is representative of a globally significant class of submarine fans in  
293 tectonically active slope basins and stepped slopes with abrupt changes in gradient (e.g.,  
294 Beaubouef and Friedmann, 2000; Sullivan et al., 2004; Beaubouef et al., 2003; Prather, 2003;  
295 Adeogba et al., 2005; Deptuck et al., 2012; Sylvester et al., 2012; Hoyal et al., 2011; 2014).

296 The geometries of our forward stratigraphic models generally match the geometries of  
297 published seismic-stratigraphic interpretations offshore of Trinidad as a result of the evolution of  
298 the surface topography alone, without the influence of other variables of the diffusion equation or  
299 changing boundary conditions, such as eustasy or subsidence. A difference between the model  
300 output and Trinidad slope fan is that thicknesses in the proximal area of the model exceed  
301 thicknesses observed in the field (Fig. 5c). This difference is likely a result of the challenge to  
302 reproduce significant sediment bypass with the limited processes used in this simplistic diffusion-  
303 based model. However, the overall trend of thinning is similar. A remaining question is whether  
304 varying other input variables can produce a similar thickness trend to the seismic-reflection  
305 interpretations while preserving patterns of compensational stacking. Future work will focus on  
306 the influence of input variables, such as erosion rates, sediment supply, sediment-gravity-flow  
307 discharge, and sediment grain-size proportion, as well as changing boundary conditions, such as  
308 tectonics and climate (e.g., Richards et al., 1998; Sømme et al., 2009; Harris et al., 2016; Hawie et  
309 al., 2017). Furthermore, future work could also compare the lithologic predictions of  
310 DionisosFlow<sup>TM</sup> to seismic attributes.

311

## 312 **Application to Reservoir Characterization and Modeling**

313 Models of slope-fan deposition from 3-D seismic-reflection data constrain the large-scale  
314 geometries of packages of strata in the subsurface; however, an important applied question is the  
315 lateral continuity and vertical connectivity of sandy and muddy architectural elements at higher  
316 resolution. These architectural elements control the static connectivity of submarine-fan reservoirs  
317 and influence fluid-flow behavior during hydrocarbon production (e.g., Glenton et al., 2013;  
318 Sutton et al., 2013). Offshore of Trinidad, the low resolution of the 3-D seismic-reflection data

319 prevented the mapping of individual channel-and-lobe architectural elements of the slope fan.  
320 Forward stratigraphic modeling provides insights into the long-term ( $>10^3$  yr) stratigraphic  
321 evolution of slope fans at high temporal and spatial resolution. In particular, the modeling provides  
322 insights into the plausible distribution of grain sizes within the slope fan.

323 Commonly used geostatistical methods in reservoir modeling use semivariograms,  
324 geometric parameters, and/or training images to reproduce spatial statistics from available  
325 conditioning data (e.g., seismic-reflection and well) and analogs, with limited use of insights from  
326 depositional processes or stratigraphic evolution (Pyrzcz and Deutsch, 2014). However, in  
327 sedimentary systems, the complex interactions of topography and flow result in erosion and  
328 deposition that govern the lateral continuity and vertical connectivity of sandy and muddy  
329 architectural elements of submarine fans (Piper and Normark, 2001). Models that fail to account  
330 for these processes might not capture realistic heterogeneity of deposits (Miller et al., 2008; Pyrcz  
331 et al., 2015).

332 Reservoir models based on integration of subsurface data (e.g., seismic-reflection,  
333 wireline-log, and core) and outcrop analogs have been shown to effectively represent heterogeneity  
334 of submarine fans. For example, Sullivan et al. (2004) produced an object-based model (Pyrzcz et  
335 al., 2015) of the A-50 reservoir of the Diana field, Gulf of Mexico deep-water slope, as proximal-  
336 to-distal channelized-to-sheet-like and layered deposits based on insights from deep-water outcrop  
337 analog data (Fig. 7c). The fundamental objects in this reservoir model were channel deposits; a  
338 large number ( $>100$ ) of these objects were initially inserted at the well locations and then inserted  
339 stochastically into interwell regions until volume (presumably net sand-to-gross stratigraphic  
340 thickness, or net-to-gross) targets were met. Figure 7 shows a net-to-gross map of the final model  
341 of Sullivan et al. (2004), which resembles the distribution of sand in a section of similar thickness

342 (~40 m maximum thickness) in our reference-case forward stratigraphic model (0.074-0.064 Ma;  
343 Fig. 7). Although the models in Figure 7 look similar, they are constructed in different ways: many  
344 conventional reservoir models are populated with a large number of channel-deposit objects so  
345 that a net-to-gross target is met, but these objects are placed without proper stratigraphic ordering  
346 and almost always without compensational stacking, whereas a diffusion-based forward  
347 stratigraphic model has proper stratigraphic ordering and realistic compensational stacking. We  
348 have shown that a relatively simple forward stratigraphic model is able to reproduce large-scale  
349 stratigraphic patterns of a submarine fan deposited across a tectonically active stepped slope.  
350 Future applied work on reservoir characterization and modeling should determine the rates of  
351 change in facies and net-to-gross within individual channel-and-lobe deposits and evaluate the  
352 impacts of sedimentologic and stratigraphic characteristics on fluid flow behavior during  
353 hydrocarbon production; particularly the 3-D stacking of architectural elements at various  
354 hierarchical scales (i.e., from individual beds to sandy and muddy architectural elements to larger-  
355 scale depocenters interpreted in seismic-reflection data; Deptuck et al., 2008) and different scales  
356 of heterogeneity depending on model time step.

357

358 **CONCLUSION**

359 We used a simple forward stratigraphic model to simulate the stratigraphic evolution of a  
360 Pleistocene submarine fan in a tectonically active slope. Our modeling results provide scenarios  
361 of the distribution of fine-scale, sub-seismic heterogeneity in the slope fan. The evolution of the  
362 surface topography, as a result of erosion and deposition, can produce the compensational-stacking  
363 patterns common in submarine fans. Varying the time step impacted the heterogeneity of the  
364 model. Shorter time steps are characterized by less sediment accumulation, which results in less



365 sediment diversion during the subsequent time step, more gradual migration of channel deposits,  
366 shorter offset distances of depocenters, and shorter length-scale heterogeneity compared to longer  
367 time steps. Thus, the controls on the compensational stacking and depocenter evolution are  
368 autogenic in these models. The processes and products of the slope fan of this study are broadly  
369 applicable to deep-water depositional systems in tectonically active slope basins. Future work will  
370 evaluate the influence of input variables and changing boundary conditions on heterogeneity of  
371 channel-and-lobe deposits of slope fans.

372

### 373 **ACKNOWLEDGMENTS**

374 We thank the sponsors of the Quantitative Clastics Laboratory (<http://www.beg.utexas.edu/qcl>).

375 We are grateful to Paradigm® for a generous donation of SeisEarth® interpretation and  
376 visualization software. We thank Lorena Moscardelli for discussions on project scope and the  
377 geology offshore Trinidad. We are grateful to Richard Sech, Morgan Sullivan, Ashley Harris, and  
378 Tao Sun for conversations regarding reservoir modeling and forward stratigraphic modeling. We  
379 thank two anonymous reviewers for recommendations that improved the clarity of this manuscript.

380

### 381 **REFERENCES CITED**

382 Adeogba, A. A., McHargue, T. R., & Graham, S. A. (2005). Transient fan architecture and  
383 depositional controls from near-surface 3-D seismic data, Niger Delta continental slope.

384 AAPG bulletin, 89(5), 627-643.

385 Alzaga-Ruiz, H., Granjeon, D., Lopez, M., Seranne, M., & Roure, F. (2009). Gravitational collapse  
386 and Neogene sediment transfer across the western margin of the Gulf of Mexico: Insights  
387 from numerical models. Tectonophysics, 470(1), 21-41.

388 Avouac, J. P., & Burov, E. B. (1996). Erosion as a driving mechanism of intracontinental mountain  
389 growth. *Journal of Geophysical Research: Solid Earth*, 101(B8), 17747-17769.

390 Beaubouef, R. T., Abreu, V., & Van Wagoner, J. C. (2003, December). Basin 4 of the Brazos–  
391 Trinity slope system, western Gulf of Mexico: the terminal portion of a late Pleistocene  
392 lowstand systems tract. In *Shelf margin deltas and linked down slope petroleum systems:  
393 Global significance and future exploration potential: Proceedings of the 23rd Annual  
394 Research Conference, Gulf Coast Section SEPM Foundation* (pp. 45-66).

395 Beaubouef, R. T., & Friedmann, S. J. (2000, December). High resolution seismic/sequence  
396 stratigraphic framework for the evolution of Pleistocene intra slope basins, western Gulf  
397 of Mexico: depositional models and reservoir analogs. In *Deep-water reservoirs of the  
398 world: Gulf Coast Section SEPM 20th Annual Research Conference* (pp. 40-60).

399 Bouma, A. H., Normark, W. R., & Barnes, N. E. (1985). *Submarine fans and related turbidite  
400 systems*. SpringerVerlag Inc., Berlin and New York.

401 Brami, T. R., Pirmez, C., Archie, C., Heeralal, S., & Holman, K. L. (2000, December). Late  
402 Pleistocene deep-water stratigraphy and depositional processes, offshore Trinidad and  
403 Tobago. In *Deep-water reservoirs of the world: Gulf Coast Section SEPM 20th Annual  
404 Research Conference* (pp. 104-115).

405 Clift, P., & Gaedicke, C. (2002). Accelerated mass flux to the Arabian Sea during the middle to  
406 late Miocene. *Geology*, 30(3), 207-210.

407 Covault, J. A., Romans, B. W., Fildani, A., McGann, M., & Graham, S. A. (2010). Rapid climatic  
408 signal propagation from source to sink in a southern California sediment-routing system.  
409 *The Journal of Geology*, 118(3), 247-259.

410 Covault, J. A., Romans, B. W., Graham, S. A., Fildani, A., & Hilley, G. E. (2011). Terrestrial  
411 source to deep-sea sink sediment budgets at high and low sea levels: Insights from  
412 tectonically active Southern California. *Geology*, 39(7), 619-622.

413 Damuth, J. E. (1994). Neogene gravity tectonics and depositional processes on the deep Niger  
414 Delta continental margin. *Marine and Petroleum Geology*, 11(3), 320-346.

415 Deptuck, M. E., Piper, D. J., Savoye, B., & Gervais, A. (2008). Dimensions and architecture of  
416 late Pleistocene submarine lobes off the northern margin of East Corsica. *Sedimentology*,  
417 55(4), 869-898.

418 Deptuck, M. E., Sylvester, Z., & O'Byrne, C. (2012). Pleistocene seascape evolution above a  
419 "simple" stepped slope, western Niger Delta. Application of the principles of seismic  
420 geomorphology to continental slope and base-of-slope systems: Case studies from sea floor  
421 and near-sea floor analog: *SEPM Special Publication*, 99, 199-222.

422 Dill, R. F., Dietz, R. S., & Stewart, H. (1954). Deep-sea channels and delta of the Monterey  
423 submarine canyon. *Geological Society of America Bulletin*, 65(2), 191-194.

424 Escalona, A., & Mann, P. (2011). Tectonics, basin subsidence mechanisms, and paleogeography  
425 of the Caribbean-South American plate boundary zone. *Marine and Petroleum Geology*,  
426 28(1), 8-39.

427 Euzen, T., Joseph, P., Du Fornel, E., Lesur, S., Granjeon, D., & Guillocheau, F. (2004). Three-  
428 dimensional stratigraphic modelling of the Grès d'Annot system, Eocene-Oligocene, SE  
429 France. *Geological Society, London, Special Publications*, 221(1), 161-180.

430 Fernandez, R. L., Cantelli, A., Pirmez, C., Sequeiros, O., & Parker, G. (2014). Growth patterns of  
431 subaqueous depositional channel lobe systems developed over a basement with a downdip  
432 break in slope: Laboratory experiments. *Journal of Sedimentary Research*, 84(3), 168-182.

433 Fildani, A., McKay, M. P., Stockli, D., Clark, J., Dykstra, M. L., Stockli, L., & Hessler, A. M.  
434 (2016). The ancestral Mississippi drainage archived in the late Wisconsin Mississippi deep-  
435 sea fan. *Geology*, 44(6), 479-482.

436 Fildani, A., & Normark, W. R. (2004). Late Quaternary evolution of channel and lobe complexes  
437 of Monterey Fan. *Marine Geology*, 206(1), 199-223.

438 Flemings, P. B., & Jordan, T. E. (1989). A synthetic stratigraphic model of foreland basin  
439 development. *Journal of Geophysical Research: Solid Earth*, 94(B4), 3851-3866.

440 French, C. D., & Schenk, C. J. (2004). Map Showing Geology, Oil and Gas Fields, and Geologic  
441 Provinces of the Caribbean Region, Open File Report 97-470-K. US Geological Survey,  
442 Denver, CO, <https://pubs.usgs.gov/of/1997/ofr-97-470/OF97-470K/index.html>.

443 Garciacaro, E., Mann, P., & Escalona, A. (2011a). Regional structure and tectonic history of the  
444 obliquely colliding Columbus foreland basin, offshore Trinidad and Venezuela. *Marine  
445 and Petroleum Geology*, 28(1), 126-148.

446 Garciacaro, E., Escalona, A., Mann, P., Wood, L., Moscardelli, L., & Sullivan, S. (2011b).  
447 Structural controls on Quaternary deepwater sedimentation, mud diapirism, and  
448 hydrocarbon distribution within the actively evolving Columbus foreland basin, eastern  
449 offshore Trinidad. *Marine and Petroleum Geology*, 28(1), 149-176.

450 Glenton, P. N., Sutton, J. T., McPherson, J. G., Fittall, M. E., Moore, M. A., Heavysege, R. G., &  
451 Box, D. (2013, March). Hierarchical approach to facies and property distribution in a basin-  
452 floor fan model, Scarborough Gas Field, North West Shelf, Australia. In IPTC 2013:  
453 International Petroleum Technology Conference.

454 Granjeon, D. (1997). Modélisation stratigraphique déterministe: conception et applications d'un  
455 modèle diffusif 3 D multilithologique. PhD dissertation, Université de Rennes.

456 Granjeon, D. (2014). 3D forward modelling of the impact of sediment transport and base level  
457 cycles on continental margins and incised valleys. *Depositional Systems to Sedimentary*  
458 *Successions on the Norwegian Continental Margin: International Association of*  
459 *Sedimentologists, Special Publication, 46, 453-472.*

460 Granjeon, D., & Joseph, P. (1999). Concepts and applications of a 3-D multiple lithology, diffusive  
461 model in stratigraphic modeling. *Numerical experiments in stratigraphy: Recent advances*  
462 *in stratigraphic and sedimentologic computer simulations: SEPM Special Publication, 62,*  
463 *197-210.*

464 Gvirtzman, Z., Csato, I., & Granjeon, D. (2014). Constraining sediment transport to deep marine  
465 basins through submarine channels: The Levant margin in the Late Cenozoic. *Marine*  
466 *Geology, 347, 12-26.*

467 Hamilton, P. B., Strom, K. B., & Hoyal, D. C. (2015). Hydraulic and sediment transport properties  
468 of autogenic avulsion cycles on submarine fans with supercritical distributaries. *Journal of*  
469 *Geophysical Research: Earth Surface, 120(7), 1369-1389.*

470 Harris, A. D., Covault, J. A., Madof, A. S., Sun, T., Sylvester, Z., & Granjeon, D. (2016). Three-  
471 Dimensional Numerical Modeling of Eustatic Control On Continental-Margin Sand  
472 Distribution. *Journal of Sedimentary Research, 86(12), 1434-1443.*

473 Hawie, N., Deschamps, R., Granjeon, D., Nader, F. H., Gorini, C., Müller, C., ... & Baudin, F.  
474 (2017). Multi-scale constraints of sediment source to sink systems in frontier basins: a  
475 forward stratigraphic modelling case study of the Levant region. *Basin Research, 29(S1),*  
476 *418-445.*

477 Heezen, B. C., Tharp, M., & Ewing, M. (1959). The floors of the oceans I. The North Atlantic.  
478 *Geological Society of America Special Papers, 65, 1-126.*

479 Hoyal, D. C. H., Demko, T., Postma, G., Wellner, R. W., Pederson, K., Abreu, V., ... & Strom, K.  
480 (2014). Evolution, architecture and stratigraphy of Froude supercritical submarine fans. In  
481 American Association of Petroleum Geologists Annual Convention and Exhibition, April  
482 (pp. 6-9).

483 Hoyal, D., Sheets, B., Wellner, R., Box, D., Sprague, A., & Bloch, R. (2011). Architecture of  
484 Froude critical-supercritical submarine fans: tank experiments versus field observations. In  
485 American Association of Petroleum Geologists Annual Convention and Exhibition, April  
486 (pp. 10-13).

487 Huyghe, P., Foata, M., Deville, E., Mascle, G., & Caramba Working Group. (2004). Channel  
488 profiles through the active thrust front of the southern Barbados prism. *Geology*, 32(5),  
489 429-432.

490 Jobe, Z. R., Sylvester, Z., Howes, N., Pirmez, C., Parker, A., Cantelli, A., ... & Prather, B. (2017).  
491 High-resolution, millennial-scale patterns of bed compensation on a sand-rich intraslope  
492 submarine fan, western Niger Delta slope. *Geological Society of America Bulletin*, 129(1-  
493 2), 23-37.

494 Lake, L. W., & Jensen, J. L. (1989). A review of heterogeneity measures used in reservoir  
495 characterization. Society of Petroleum Engineers.

496 Leonard, R. (1983). Geology and hydrocarbon accumulations, Columbus Basin, offshore Trinidad.  
497 AAPG Bulletin, 67(7), 1081-1093.

498 McHargue, T., Pyrcz, M. J., Sullivan, M. D., Clark, J. D., Fildani, A., Romans, B. W., ... &  
499 Drinkwater, N. J. (2011). Architecture of turbidite channel systems on the continental  
500 slope: patterns and predictions. *Marine and Petroleum Geology*, 28(3), 728-743.

501 Menard Jr, H. W. (1955). Deep-sea channels, topography, and sedimentation. AAPG Bulletin,  
502 39(2), 236-255.

503 Miller, J. K., Sun, T., Li, H., Stewart, J., Genty, C., Li, D., & Lyttle, C. (2008, January). Direct  
504 modeling of reservoirs through forward process-based models: Can we get there?. In  
505 International petroleum technology conference. International Petroleum Technology  
506 Conference.

507 Mize, K. L. (2004). Controls on the morphology and development of deep-marine channels,  
508 Eastern Offshore Trinidad and Venezuela. MS dissertation, The University of Texas at  
509 Austin.

510 Moscardelli, L. G. (2007). Mass transport processes and deposits in offshore Trinidad and  
511 Venezuela, and their role in continental margin development. PhD dissertation, The  
512 University of Texas at Austin.

513 Moscardelli, L., & Wood, L. (2008). New classification system for mass transport complexes in  
514 offshore Trinidad. Basin research, 20(1), 73-98.

515 Moscardelli, L., Wood, L., & Mann, P. (2006). Mass-transport complexes and associated processes  
516 in the offshore area of Trinidad and Venezuela. AAPG bulletin, 90(7), 1059-1088.

517 Moscardelli, L., Wood, L. J., & Dunlap, D. B. (2012). Shelf-edge deltas along structurally complex  
518 margins: a case study from eastern offshore Trinidad. AAPG bulletin, 96(8), 1483-1522.

519 Mutti, E., & Normark, W. R. (1987). Comparing examples of modern and ancient turbidite  
520 systems: problems and concepts. In Marine clastic sedimentology (pp. 1-38). Springer  
521 Netherlands.

522 Normark, W. R., Posamentier, H., & Mutti, E. (1993). Turbidite systems: state of the art and future  
523 directions. Reviews of Geophysics, 31(2), 91-116.

524 Patterson, M. B., Blom, F., Griffith, C. M., Tepper, B. J., & Truempy, D. (2001). Sweet Music in  
525 the Columbus Basin: From Mozart to Haydn, and Then? In American Association of  
526 Petroleum Geologists Annual Convention and Exhibition, June.

527 Pettingill, H. S., & Weimer, P. (2002). Worldwide deepwater exploration and production: Past,  
528 present, and future. *The Leading Edge*, 21(4), 371-376.

529 Piper, D. J., & Normark, W. R. (2001). Sandy fans--from Amazon to Hueneme and beyond. *AAPG*  
530 *bulletin*, 85(8), 1407-1438.

531 Pinheiro-Moreira, J. L. (2000). Stratigraphie sismique et modélisation stratigraphique des dépôts  
532 de l'Éocène du Bassin de Santos (marge brésilienne). PhD dissertation, Université de  
533 Rennes.

534 Pirmez, C., Beaubouef, R. T., Friedmann, S. J., & Mohrig, D. C. (2000, December). Equilibrium  
535 profile and baselevel in submarine channels: examples from Late Pleistocene systems and  
536 implications for the architecture of deepwater reservoirs. In *Global deep-water reservoirs:*  
537 *Gulf Coast Section SEPM Foundation 20th Annual Bob F. Perkins Research Conference*  
538 (pp. 782-805).

539 Postma, G., Hoyal, D. C., Abreu, V., Cartigny, M. J., Demko, T., Fedele, J. J., ... & Pederson, K.  
540 H. (2016). Morphodynamics of supercritical turbidity currents in the channel-lobe  
541 transition zone. In *Submarine Mass Movements and their Consequences* (pp. 469-478).  
542 Springer International Publishing.

543 Prather, B. E. (2003). Controls on reservoir distribution, architecture and stratigraphic trapping in  
544 slope settings. *Marine and Petroleum Geology*, 20(6), 529-545.

545 Prather, B. E., Pirmez, C., & Winker, C. D. (2012). Stratigraphy of linked intraslope basins:  
546 Brazos-Trinity system western Gulf of Mexico. *Application of the Principles of Seismic*



547 Geomorphology to Continental-Slope and Base-of-Slope Systems: Case Studies from  
548 Seafloor and Near-Seafloor Analogues: SEPM, Special Publication, 99, 83-110.

549 Prélat, A., Covault, J. A., Hodgson, D. M., Fildani, A., & Flint, S. S. (2010). Intrinsic controls on  
550 the range of volumes, morphologies, and dimensions of submarine lobes. *Sedimentary*  
551 *Geology*, 232(1), 66-76.

552 Prélat, A., Hodgson, D. M., & Flint, S. S. (2009). Evolution, architecture and hierarchy of  
553 distributary deep-water deposits: a high-resolution outcrop investigation from the Permian  
554 Karoo Basin, South Africa. *Sedimentology*, 56(7), 2132-2154.

555 Pyrcz, M. J., & Deutsch, C. V. (2014). *Geostatistical reservoir modeling*. Oxford university press.

556 Pyrcz, M. J., Sech, R. P., Covault, J. A., Willis, B. J., Sylvester, Z., & Sun, T. (2015). Stratigraphic  
557 rule-based reservoir modeling. *Bulletin of Canadian Petroleum Geology*, 63(4), 287-303.

558 Rabineau, M., Berné, S., Aslanian, D., Olivet, J. L., Joseph, P., Guillocheau, F., ... & Granjeon, D.  
559 (2005). Sedimentary sequences in the Gulf of Lion: a record of 100,000 years climatic  
560 cycles. *Marine and Petroleum Geology*, 22(6), 775-804.

561 Richards, M., Bowman, M., & Reading, H. (1998). Submarine-fan systems I: characterization and  
562 stratigraphic prediction. *Marine and Petroleum Geology*, 15(7), 689-717.

563 Rowan, M. G., Peel, F. J., & Vendeville, B. C. (2004). Gravity-driven fold belts on passive  
564 margins. *AAPG Memoir*, 82, 157-182.

565 Ryan, W. B., Carbotte, S. M., Coplan, J. O., O'Hara, S., Melkonian, A., Arko, R., ... &  
566 Bonczkowski, J. (2009). Global multi-resolution topography synthesis. *Geochemistry,*  
567 *Geophysics, Geosystems*, 10(3).

568 Shepard, F. P. & Emery, K. O. (1941). Submarine topography off the California coast: Canyon  
569 and tectonic interpretation. *Geological Society of America Special Papers*, 31, 1-171.

570 Sømme, T. O., Helland-Hansen, W., & Granjeon, D. (2009). Impact of eustatic amplitude  
571 variations on shelf morphology, sediment dispersal, and sequence stratigraphic  
572 interpretation: Icehouse versus greenhouse systems. *Geology*, 37(7), 587-590.

573 Spinewine, B., Sequeiros, O. E., Garcia, M. H., Beaubouef, R. T., Sun, T., Savoye, B., & Parker,  
574 G. (2009). Experiments on wedge-shaped deep sea sedimentary deposits in minibasins  
575 and/or on channel levees emplaced by turbidity currents. Part II. Morphodynamic evolution  
576 of the wedge and of the associated bedforms. *Journal of Sedimentary Research*, 79(8), 608-  
577 628.

578 Sullivan, S. M. (2005). *Geochemistry, sedimentology, and morphology of mud volcanoes, eastern*  
579 *offshore Trinidad*. MS dissertation, The University of Texas at Austin.

580 Sullivan, M. D., Foreman, J. L., Jennette, D. C., Stern, D., Jensen, G. N., & Goulding, F. J. (2004).  
581 An integrated approach to characterization and modeling of deep-water reservoirs, Diana  
582 field, western Gulf of Mexico. *AAPG Memoir*, 80, 215-234.

583 Sullivan, M., Jensen, G., Goulding, F., Jennette, D., Foreman, L., & Stern, D. (2000, December).  
584 Architectural analysis of deep-water outcrops: Implications for exploration and  
585 development of the Diana sub-basin, western Gulf of Mexico. In *Deep-water reservoirs of*  
586 *the world: Gulf Coast Section SEPM Foundation 20th Annual Research Conference* (pp.  
587 1010-1032).

588 Sun, T., Ghayour, K., Hall, B., & Miller, J. (2010, December). Process-based modeling of deep  
589 water depositional systems. In *Seismic Imaging of Depositional and Geomorphic Systems:*  
590 *Gulf Coast Section SEPM Foundation 30th Annual Bob F. Perkins Research Conference*  
591 (pp. 88-112).

592 Sutton, J. T., Glenton, P. N., Fittall, M. E., Moore, M. A., & Box, D. (2013, March). Reservoir  
593 Simulation to Investigate the Effect of Flow Baffles in a Basin-Floor Fan, Scarborough  
594 Field, North West Shelf, Australia. In SPE Middle East Oil and Gas Show and Conference.  
595 Society of Petroleum Engineers.

596 Sylvester, Z., Deptuck, M. E., Prather, B. E., Pirmez, C., & O'Byrne, C. (2012). Seismic  
597 stratigraphy of a shelf-edge delta and linked submarine channels in the northeastern Gulf  
598 of Mexico. Application of the Principles of Seismic Geomorphology to Continental-Slope  
599 and Base-of-Slope Systems: Case Studies from Seafloor and Near-Seafloor Analogues:  
600 SEPM, Special Publication, 99, 31-59.

601 Tucker, G. E., & Slingerland, R. L. (1994). Erosional dynamics, flexural isostasy, and long-lived  
602 escarpments: A numerical modeling study. *Journal of Geophysical Research: Solid Earth*,  
603 99(B6), 12229-12243.

604 Weber, J. C., Dixon, T. H., DeMets, C., Ambeh, W. B., Jansma, P., Mattioli, G., ... & Pérez, O.  
605 (2001). GPS estimate of relative motion between the Caribbean and South American plates,  
606 and geologic implications for Trinidad and Venezuela. *Geology*, 29(1), 75-78.

607 Willgoose, G., Bras, R. L., & Rodriguez-Iturbe, I. (1991). A coupled channel network growth and  
608 hillslope evolution model: 1. Theory. *Water Resources Research*, 27(7), 1671-1684.

609 Wood, L. J., & Mize-Spansky, K. L. (2009). Quantitative seismic geomorphology of a Quaternary  
610 leveed-channel system, offshore eastern Trinidad and Tobago, northeastern South  
611 America. *AAPG Bulletin*, 93(1), 101-125.

612

613 **FIGURE CAPTIONS**

614 Figure 1. Example of Brazos-Trinity Basin II slope-fan depositional architecture. a. Co-rendered  
615 bathymetry and slope of Basin II from the BOEM Northern Gulf of Mexico Deepwater  
616 Bathymetry Grid from 3D Seismic ([https://www.boem.gov/Gulf-of-Mexico-Deepwater-  
617 Bathymetry/](https://www.boem.gov/Gulf-of-Mexico-Deepwater-Bathymetry/)). b. Isochron map of the Upper Sequence. c. Upper Sequence stratigraphic  
618 architecture. d. Isochron maps of mass-transport complex, distributary channel-lobe  
619 complex, and leveed-channel complex of the Upper Sequence. Parts b-d modified from  
620 Beaubouef and Friedmann (2000).

621 Figure 2. Caribbean geologic setting. Bathymetry is from Geomapapp.org (Ryan et al., 2009).  
622 Faults are black lines (French and Schenk, 2004).

623 Figure 3. Co-rendered bathymetry and slope offshore Trinidad. Modified from Mize (2004),  
624 Sullivan (2005), Moscardelli and Wood (2008), and Wood and Mize-Spansky (2009).

625 Figure 4. a-b. Time-structure maps of base and top of a slope fan. a. Base of the slope fan is the  
626 initial bathymetry of the stratigraphic forward model (Top MTC\_1 horizon of Moscardelli  
627 et al., 2006). b. Top of the slope fan is the seafloor (Mize, 2004; Sullivan, 2005; Moscardelli  
628 and Wood, 2008; Wood and Mize-Spansky, 2009). c. Isochron map of the slope fan from  
629 Moscardelli et al. (2006) and Moscardelli and Wood (2008).

630 Figure 5. Reference-case model (10 kyr time step). a. Isochore map of the entire model. b. Sand  
631 percentage map, calculated based on the proportion of coarse- and medium-grained sand.  
632 c. Difference between the thickness of the model and the thickness of the slope fan in block  
633 25A, assuming a sound velocity of 2000 m/s. d. Grain-size distribution at 0.104, 0.064, and  
634 0.034 time steps. e. Isochore maps of depositional sequences within the model showing  
635 major phases of sediment diversion. f. Cross sections of the model. Left (L) and right (R)

636 orientations in cross sections are left and right in maps in parts a-e. Locations shown in  
637 part d. See Supplementary Files 1-2 for the detailed stratigraphic evolution.

638 Figure 6. Isochore and sand percentage maps and cross sections of the 20 kyr time-step model (a),  
639 the 5 kyr time-step model (b), and the 1 kyr time-step model (c). Left (L) and right (R)  
640 orientations in cross sections are left and right in maps. Cross-section locations shown in  
641 part a. See Supplementary Files 3-8 for the detailed stratigraphic evolution.

642 Figure 7. Sand percentage map of reference-case model (10 kyr time step) of the sequence  
643 deposited between 0.074-0.064 Ma (a-b) compared to the object-based model of the A-50  
644 reservoir of the Diana field, Gulf of Mexico deep-water slope (c). In part c, net-to-gross  
645 ranges from  $> 0.95$  in the proximal area (red) to  $< 0.40$  in the distal area (purple). Part c  
646 modified from Sullivan et al. (2004).

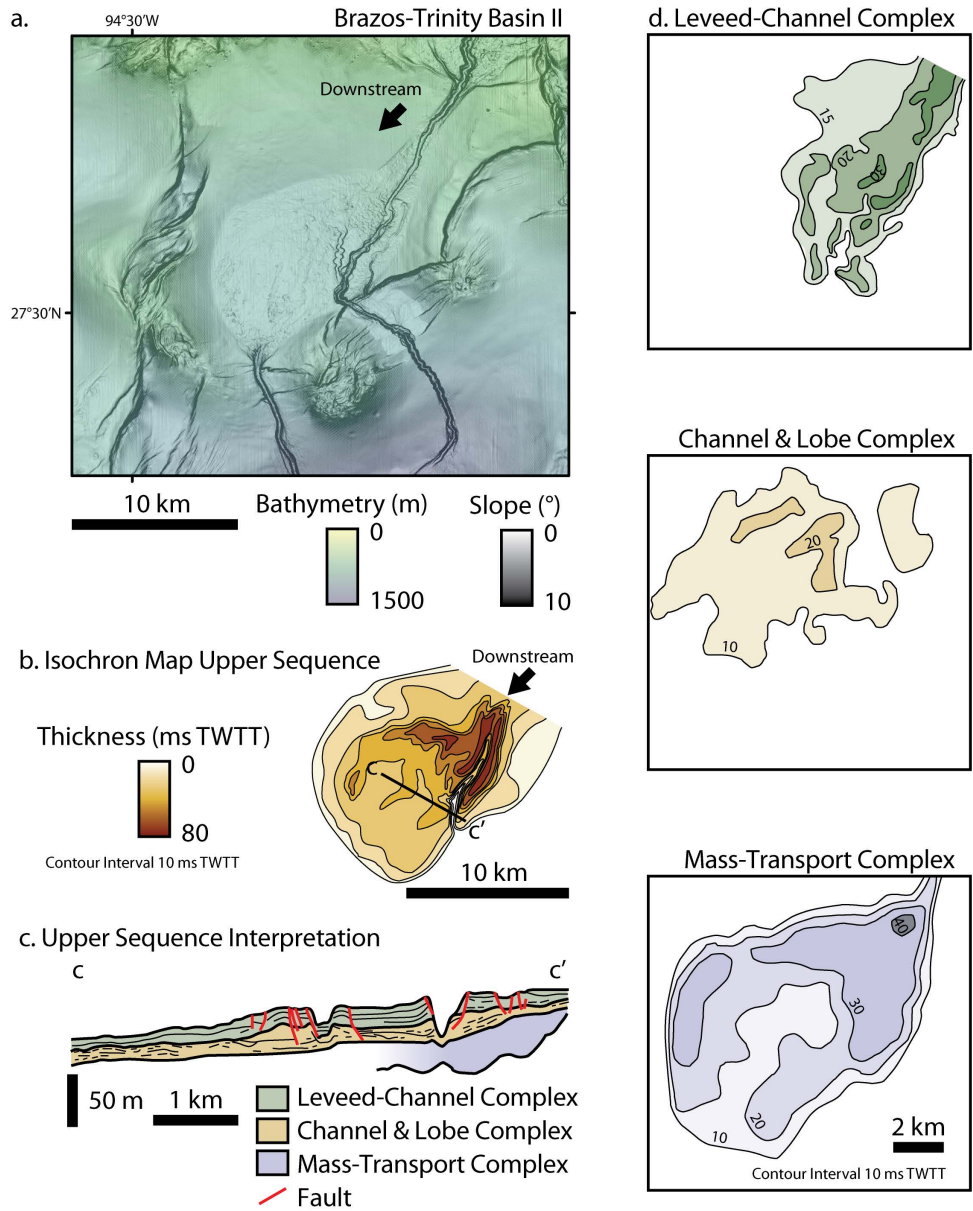


Figure 1

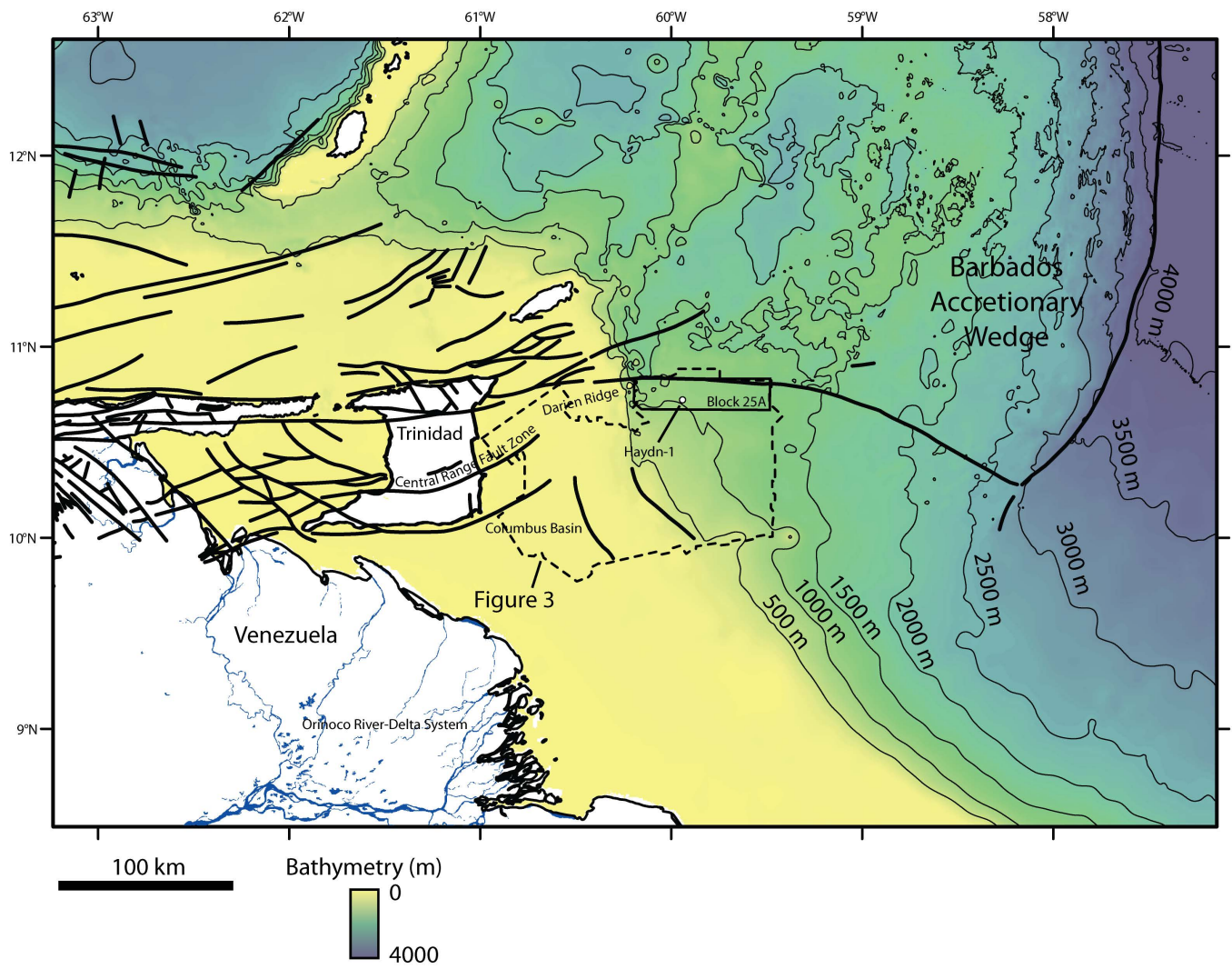


Figure 2

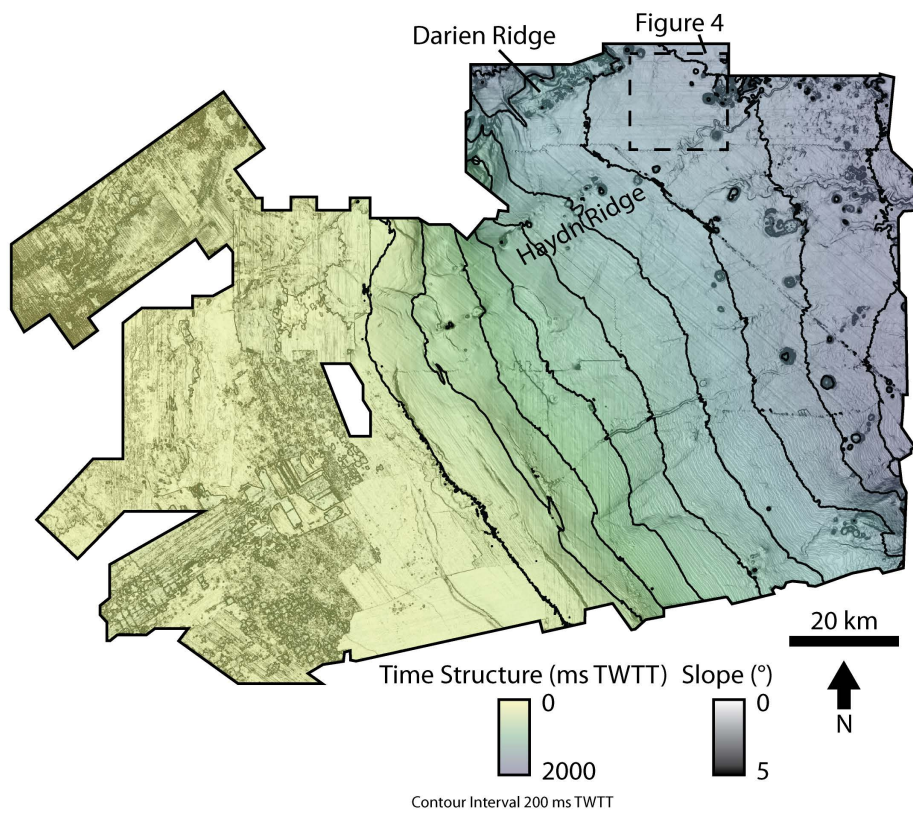


Figure 3



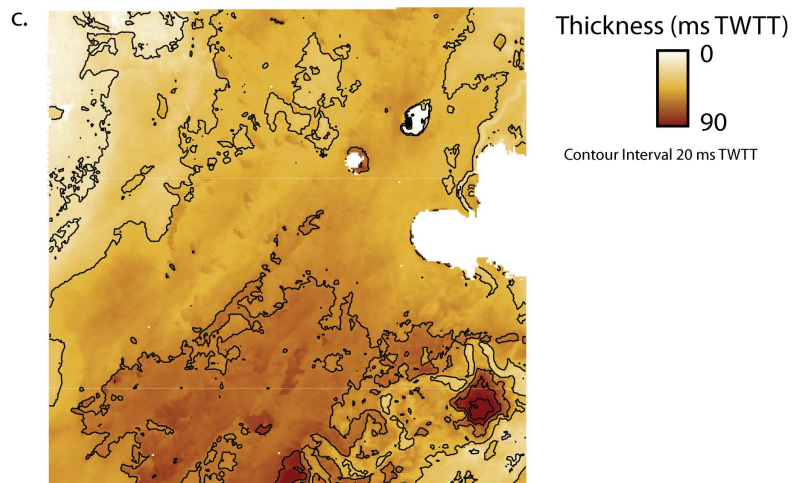
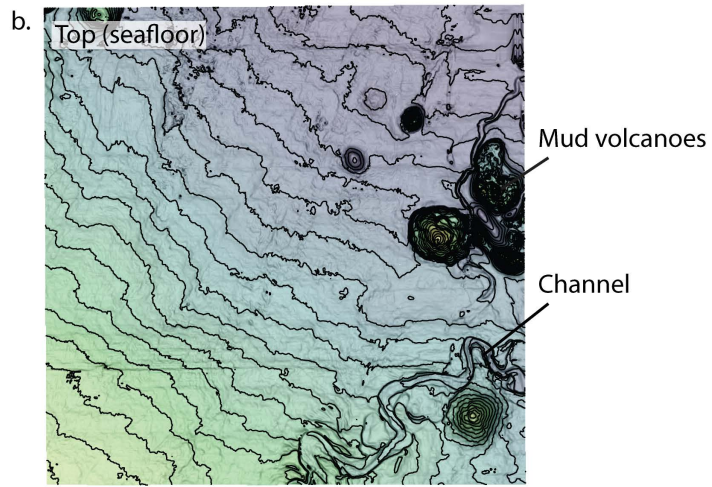
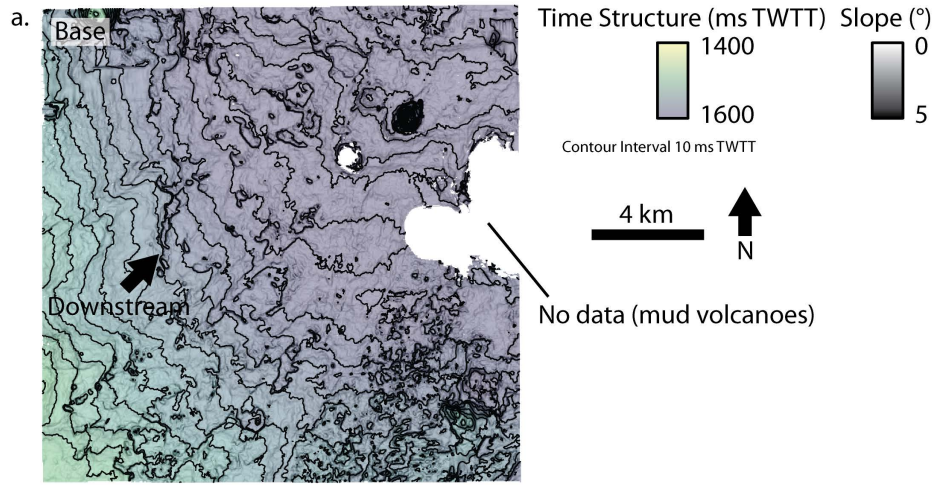


Figure 4

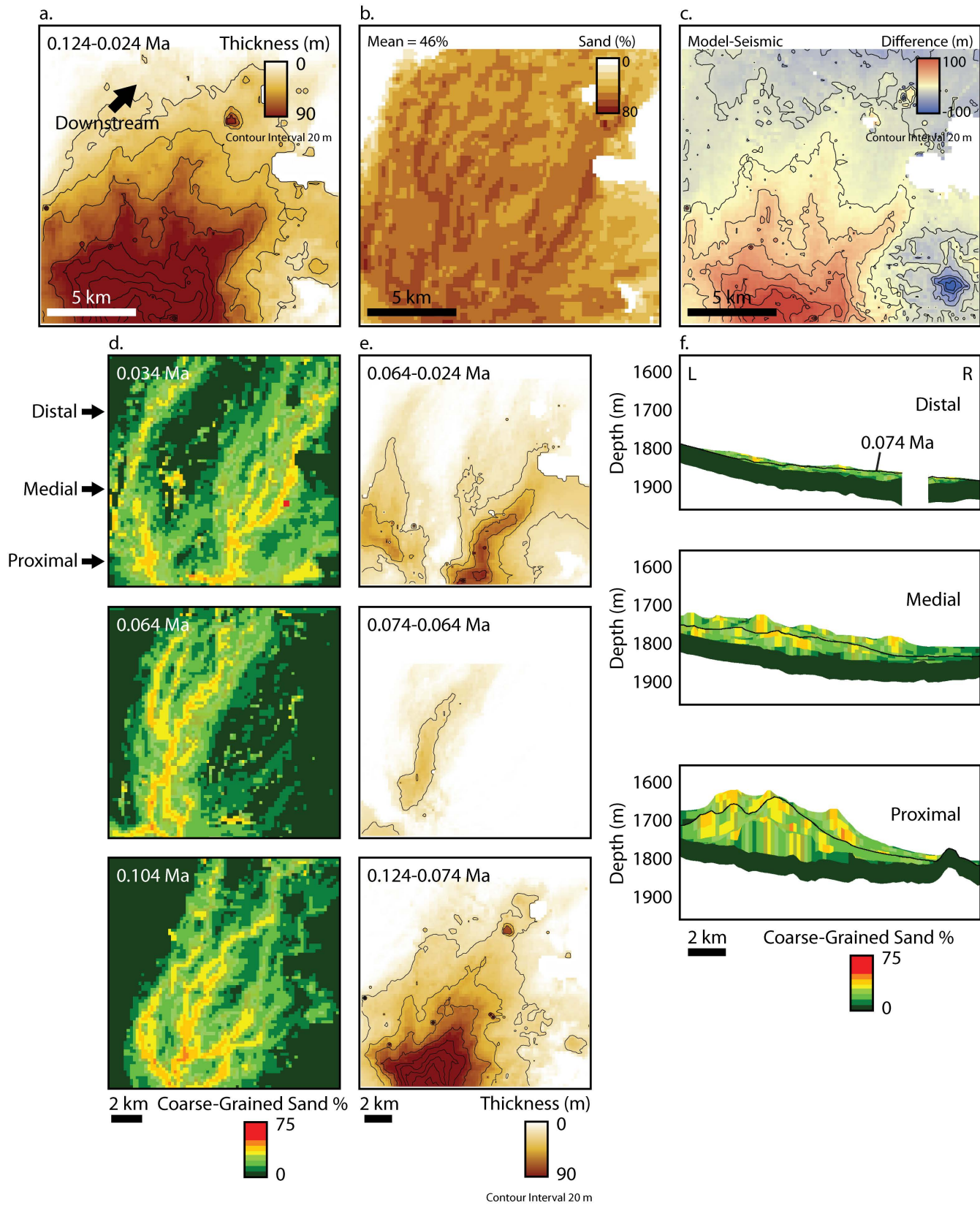


Figure 5

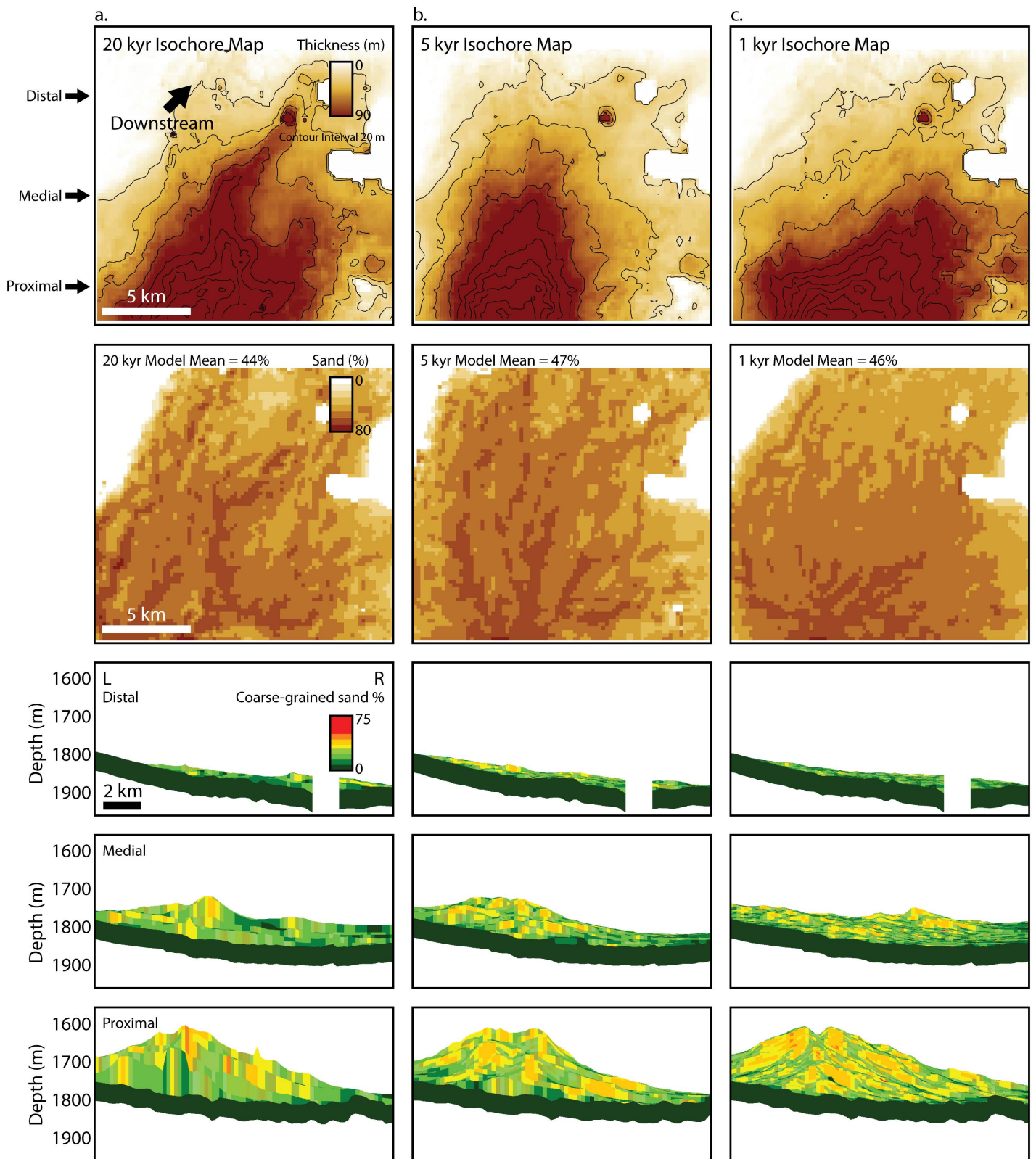


Figure 6

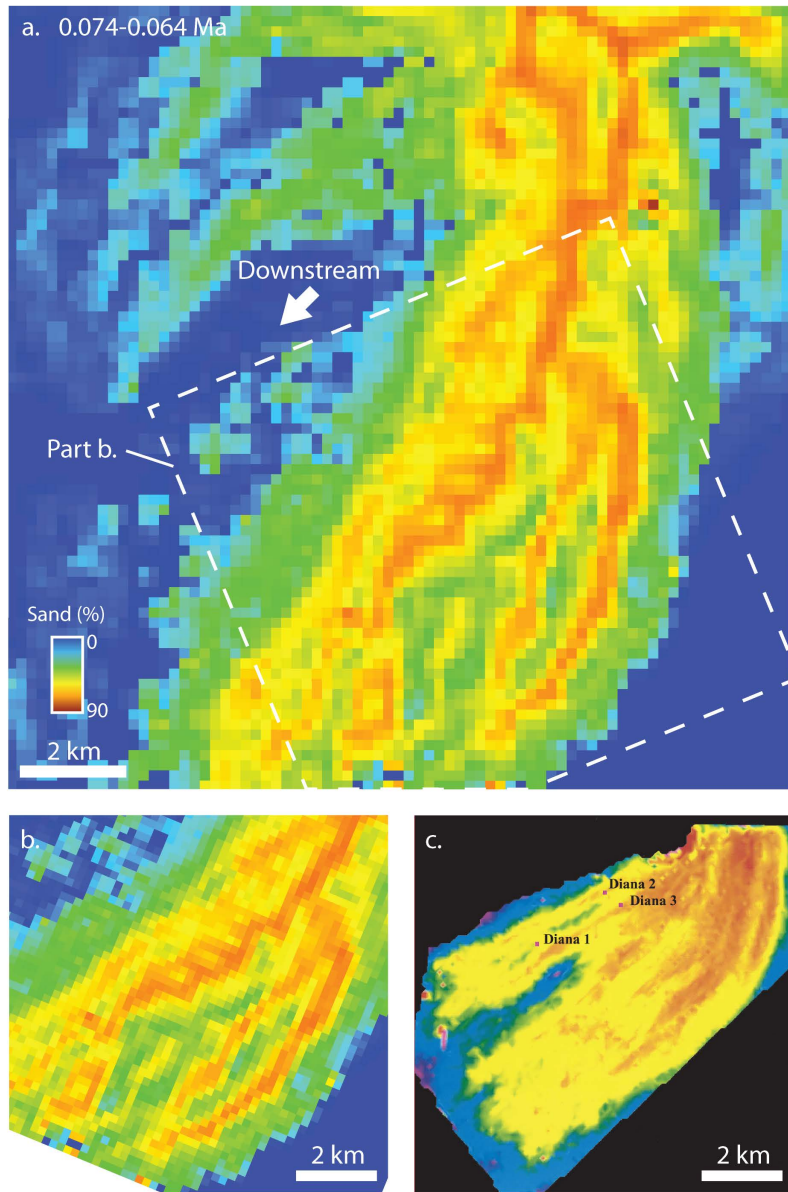


Figure 7